Low-Dose Imaging Performance of a Clinical Organ-Targeted Positron Emission Tomography (PET) Camera

Brandon Baldassi
Department of Physics, Lakehead University, Thunder Bay, Canada

Oleksandr Bubon
Department of Physics, Lakehead University, Thunder Bay, Canada
Thunder Bay Regional Health Research Institute, Thunder Bay, Canada
Radialis Inc., Thunder Bay, Canada

Justin Stiles, Harutyun Poladyan
Department of Physics, Lakehead University, Thunder Bay, Canada

Vivianne Freitas, Anabel Scaranelo
University Health Network, Women's College Hospital, Toronto, Ontario, Canada
University of Toronto, Toronto, Ontario, Canada

Borys Komarov
Department of Computer Science, Lakehead University, Thunder Bay, Canada

Michael Waterston
Radialis Inc., Thunder Bay, Canada

Alla Reznik
Department of Physics, Lakehead University, Thunder Bay, Canada
Thunder Bay Regional Health Research Institute, Thunder Bay, Canada

Introduction

Despite the proven value of molecular imaging in diagnostic procedures across clinical applications, the standard radiotracer doses associated with PET limit the potential for use in undiagnosed patients for screening applications and in radiation-sensitive populations. [1] Additionally, conventional whole-body (WB) PET is limited in detection of small lesions characteristic of early-stage cancer, delaying diagnosis and potential treatment options.

In this regard, attention is currently being paid to techniques which may produce high-quality PET images using a low dose of radiotracer, both from post-processing of input images acquired with a reduced dose, and with improved PET detector hardware for more efficient collection of emitted gamma photons. [2] Improved sensitivity and image quality associated with organ-targeted PET will allow clinicians to resolve lesions using less radioactivity. This enhances diagnostic capabilities while minimizing the dose to the patient - an important element in improving accessibility of PET procedures to wider populations.

The organ-targeted PET technology described herein focuses precisely on the matter of hardware-based improvements in detection sensitivity and imaging quality. This is achieved through detector design and increased geometric coverage by arranging large FOV detectors proximal to the specific organ of interest. The first application of the developed technology is for imaging in breast with the Radialis PET camera.

PET Camera

Radialis PET camera employs two planar detector heads, each comprised of seamless arrays of sensor modules to produce a large field of view comparable to X-ray mammography. [3] The detectors are mounted on a movable gantry which permits rotation, relative translation, and overall height adjustment to accommodate imaging for a variety of indications. Image reconstruction is performed on list-mode data using the system's clinical 3D-MLEM GPU-based algorithm with 15 iterations.

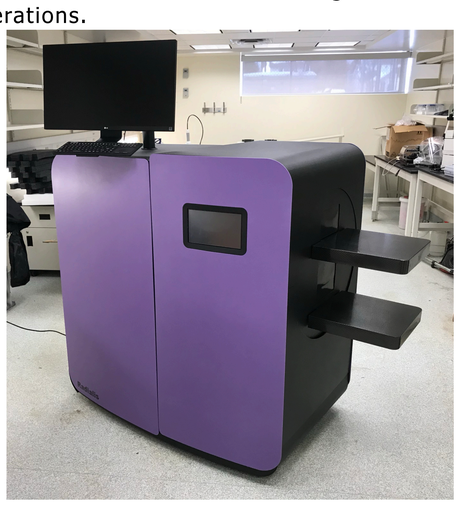

Figure 1. The Radialis PET Camera system with two position-adjustable planar detectors.

Detector Technology

- Each detector comprises 12 four-side tileable (mosaic) sensor modules that are arranged in a 3x4 array producing a seamless imaging area of 23 x 17 cm^2.
- Detector modules (58×58 mm^2) consist of pixelated LYSO crystals coupled to silicon-based photosensors (SiPM). The SiPMs have a matrix of 8×8 pixels which are multiplexed into a 4-channel signal readout.
- An uncoated 5 mm thick Borosilicate light guide optically couples the scintillation crystals and SiPMs while permitting light sharing over multiple SiPM pixels.
- Imaging area is only 4 mm from the detector enclosure resulting in minimal dead-zone.

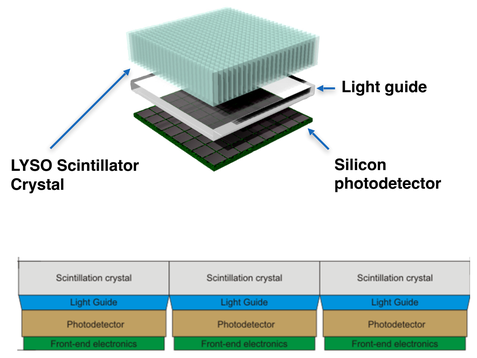

Figure 2. Schematic representation of detector modules used in the PET camera (top) and diagram of seamless arrangement (bottom).

Property	Radialis PET Camera
Detector configuration	Planar arrays
Scintillation crystal	LYSO:Ce
Crystal size, (mm^3)	2.32 × 2.32 × 13
Crystal pitch (mm)	2.4
Crystal size array	24 × 24
Photosensor array	Si-PM, Sensl, C-series 8x8
# of detector modules	24
Total # of crystals	13,824
# of readout channels	96
Number of ADCs	6
Coincidence timing window (ns)	4
Energy window (keV)	350 - 700
Angle allowance (rad)	1
FOV (mm)	172 × 232
Axial FOV (mm)	45 – 250

Table 1. Selected specifications of the Radialis PET camera.

Figure 3. Schematic of the two detectors showing the imaging field of view and arrangement of axes, with the axial plane is aligned with Z axis direction.

Detector Performance

Radialis detectors are placed on both sides of the immobilized breast for (1) more efficient gamma-ray detection and (2) reduced unwanted signal from elsewhere in the body, improving the noise equivalent count rate (NECR) within the field of view (FOV) due to a reduction of false coincidences. Combined with seamless PET detector technology and high-gain photosensors, the result is highly efficient activity detection. The measured peak NECR is 17.8 kcps at a ^{18}F-FDG concentration of 10.5 kBq/mL. The maximum axial sensitivity is 3.5% with an average system sensitivity of 2.4%. Both the efficiency at peak count rate (Table 2) and sensitivity (Figure 4) exceed that of any WB or organ-targeted PET scanner on the market or in clinical trials.

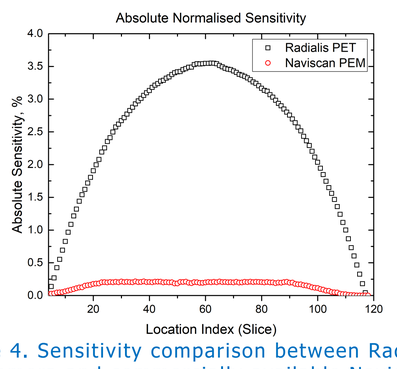

Figure 4. Sensitivity comparison between Radialis PET camera and commercially available Naviscan Positron Emission Mammography (PEM) Flex Solo II [4]

Selected clinical images (Figures 4-6) from the clinical trials (ClinicalTrials.gov ID: NCT03520218) are shown for breast cancer patients who underwent full-field digital mammogram (FFDM) and gadolinium-enhanced breast MRI, in addition to an organ-targeted PET scan with standard or low radiotracer dose.

Low-dose Imaging

PET System	Efficiency at Peak Count Rate (cps/MBq)	Peak NECR (kcps)	Concentration at Peak NECR (kBq/mL)	Phantom Volume (mL)	Activity at Peak NECR (MBq)
Radialis PET Camera	5,650	17.8	10.5	300	3.15
uExplorer (Total Body)	3,790	1440	16.8	22,600	380
Oncovision Mammi PEM Dual Ring	1,260	34.0	31.2	866	27.0
GE Discovery IQ (PET/CT)	618	123.6	9.1	22,000	200
GE Discovery MI (PET/CT)	581	266	20.8	22,000	458
Phillips Vereos (PET/CT)	556	646	52.8	22,000	1,160
GE Signa PET (PET/MR)	524	218	17.8	22,600	402
Siemens Biograph Vision (PET/CT)	435	306	32	22,000	704
Naviscan PEM Flex Solo II (PEM)	393	10.6	90	300	27.0

Table 2. Count rate data for several organ-targeted, whole-body and emerging total-body PET systems obtained through standardized phantom measurements. [2] Values for efficiency at peak count rate are calculated from the peak NECR data reported for each system.

Standardized phantom measurements and acquisition of clinical images indicate the ability to resolve lesions obscured in X-ray mammography even at 1/10th of the standard clinical dose.

The low-dose Radialis PET imaging at radiation exposure suitable for screening applications shows high breast cancer specificity and potential for correcting of both false-negative findings with x-ray mammography and digital breast tomosynthesis, and false-positive findings in breast MRI.

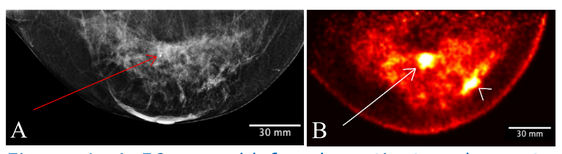

Figure 4: A 56-year-old female patient underwent FFDM imaging (A) with red arrow indicating the site of a primary lesion. Organ-targeted PET image (B) with 37 MBq ^{18}F-FDG injection and same craniocaudal (CC) view shows two distinct sites of contrast enhancement. The second site (arrowhead) is not detected in mammography. Both sites were confirmed cancerous by histopathology.

Lesion properties	Primary lesion	Secondary lesion
Volume (mL)	0.14	0.11
Mean SUV$_{LBM}$ (g/mL)	5.3	5.3
Maximum SUV$_{LBM}$ (g/mL)	12.2	10.7
Minimum SUV$_{LBM}$ (g/mL)	2.0	2.0
Total lesion glycolysis (g)	0.73	0.60

Table 3. Quantified lesion properties from the organ-targeted PET scan.

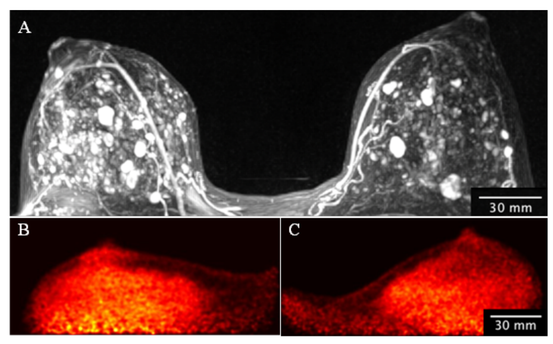

Figure 5: A 33-year-old high-risk female underwent pre-operative breast MRI with multiple enhancing masses noted in the 3D-MIP image (A) and without corresponding masses noted in the organ-targeted PET images (B) with a 43 MBq ^{18}F-FDG injection. The MLO views from the Radialis PET Camera are presented for the left (B) and right (C) side without evident focal ^{18}F-FDG uptake in either image. The surgical pathology results do not show signs of cancer.

Quantification and Feature Extraction

In the era of precision and personalized medicine, disease detection is only the beginning of the clinical pathway for patients. Quantification of tumour metabolic properties is becoming the predominant means of assessing treatment efficacy and surgical completeness. Selected clinical images are presented in Figure 6 for a breast cancer patient who underwent an organ-targeted PET scan from which a 3-D model representative of abnormal tissue metabolism is derived. The results demonstrate capabilities in not only visualizing the spatial distribution of abnormally metabolic tissue, but also in quantifying its properties and extracting precise physical features which are needed in applications such as neoadjuvent chemotherapy, treatment follow-ups, and post-surgical assessment.

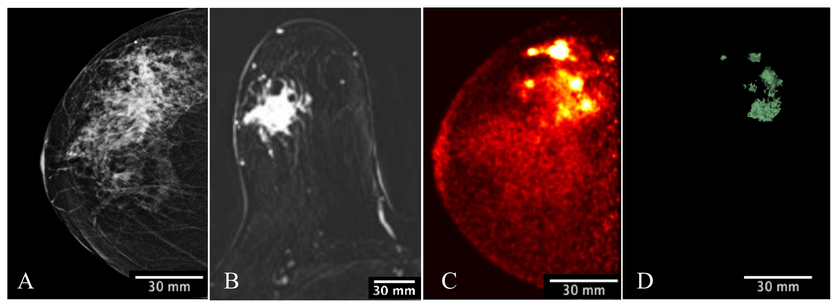

Lesion properties	Measured values
Volume (mL)	2.4
Mean SUV$_{LBM}$ (g/mL)	1.8
Maximum SUV$_{LBM}$ (g/mL)	3.4
Minimum SUV$_{LBM}$ (g/mL)	1.5
Total lesion glycolysis (g)	4.4

Table 4. Quantified lesion properties from the organ-targeted PET scan.

Figure 6: A 61-year-old female with right-breast multifocal invasive and in situ ductal carcinoma. Images of the same breasts in (A) FFDM in the CC plane showing extensive distortion, (B) a selected slice of MRI in the axial plane showing irregular shape-enhancing lesion 2 min post gadolinium-chelate-based contrast administration, (C) Radialis PET in the CC plane showing multiple distinct regions of contrast uptake 3 h after injection of 178 MBq 18F-FDG, (D) 3-D volume generated from Radialis PET in the CC plane based upon tissue metabolism threshold across all image slices.

Summary

The organ-targeted PET system shows an improved ability to resolve lesions which may be obscured or lead to false-negative findings in mammography. Clinical demonstration with imaging in breast revealed that the Radialis PET camera is well-suited to identifying breast cancers even at a 10-fold dose reduction in comparison with standard WB PET dose. We also demonstrate the ability to address the high false-positive rate associated with breast MRI and a well-known problem of breast cancer over-diagnosis with breast MRI [6-7]. The system performance is quantified and outperforms commercially available breast-dedicated PET and WB PET systems in terms of overall efficiency and best-in-class sensitivity. Finally, we demonstrate the possibility to extract precise metabolic data which may inform treatment response and disease staging in emerging applications such as neoadjuvant chemotherapy.

Acknowledgement

The authors are indebted to Sergey Reznik and Giovanni DeCrescenzo for technical support. Financial support from the Ontario Research Fund – Research Excellence program, Natural Sciences and Engineering Research Council of Canada, Canadian Breast Cancer Foundation, Northern Ontario Heritage Fund Corporation and Radialis is gratefully acknowledged.

References

[1] Jones, T., Townsend, D.W. History and future technical innovation in positron emission tomography, J. Med. Imag., 2017; 4(1) 011013.

[2] Catana, C. The Dawn of a New Era in Low-Dose PET Imaging, Radiology, 2019; 290, 657–658.

[3] Reznik, A., Bubon, O., Teymurazyan, A. Tileable block detectors for seamless block detector arrays in Positron Emission Mammography, 2017; Patent WO2017/143442A1. World Intellectual Property Org.

[4] Stiles, J., Baldassi, B., Bubon, O., Poladyan, H., Freitas, V., Scaranelo, A., Mulligan, A.M., Waterston, M., Reznik, A. Evaluation of a High-Sensitivity Organ-Targeted PET Camera, Sensors. 2022; 22(13):4678.

[5] Luo, W., Anashkin, E. & Matthews, C. G., Performance evaluation of a PEM scanner using the NEMA NU 4-2008 small animal PET standards, IEEE Trans. Nucl. Sci, 2010; 57, 94–103.

[6] Narod, S. The importance of overdiagnosis in breast-cancer screening. Nature Rev Clin Oncol. 2016; 13, 5–6.

[7] Evans, A., Vinnicombe, S. Overdiagnosis in breast imaging. Breast. 2017; Feb;31:270-273